PHYSOR 2004 -The Physics of Fuel Cycles and Advanced Nuclear Systems: Global Developments
Chicago, Illinois, April 25-29, 2004, on CD-ROM, American Nuclear Society, Lagrange Park, IL. (2004)

Verification of Lattice Analysis Method through BWR UO_2 PIE Data Analysis

T. Yamamoto* and K. Kawashima
Japan Nuclear Energy Safety Organization, Fujita Kanko Toranomon Bldg., 3-17-1, Toranomon, Minato-ku, Tokyo, 105-0001, Japan

Calculations with a lattice analysis code have been done for the experimental data of the rod-by-rod distributions of FP nuclides in the BWR fuel assemblies with the burn up form 12.6 to 48.8 GWd/t and for the pellet average isotope compositions of actinide nuclides (U, Pu, Am and Cm) and major FP nuclides with the pellet burn up from 16.7 to 44.0 GWd/t. The experimental data are those for the 8x8 UO2 fuel assemblies that were discharged from the Unit 2 of Fukushima power station 2 (2F2).

The SRAC cord system coupled with the JENDL-3.2 nuclear data library has been used for the burn-up calculations. For the rod-by-rod distributions of the FP nuclide, the values of C-E (%) are from 0 to 4 % except for the Gd2O3-UO2 fuel rod. The root mean square of the difference between the analysis results and the measurements of the 7-rod positions is almost in two times of the statistical errors of the measurements. For the pellet average isotope compositions of actinide nuclides, the comparison between the analysis and measurement results has been done and discussed in terms of the measurement errors and analysis methods.

KEYWORDS: BWR, 8x8 fuel assembly, PIE, FP nuclide, rod-by-rod distribution, actinide nuclide, pellet average isotope composition, lattice analysis, SRAC cord, JENDL-3.2

1. Introduction

Utilizing plutonium as mixed-oxide (MOX) fuel in commercial light water reactors is one of the nuclear energy policies of Japan. The nearest milestone is to load MOX fuel up to one third of the core (1/3 MOX core) in commercial LWRs. The utilities are planning to introduce MOX in 16 to 18 commercial LWR units by 2010. Moreover, in order to enhance the flexibility of the MOX fuel utilization, it is scheduled to introduce a full MOX core for an Advanced Boiling Water Reactor (Full MOX ABWR). It has been verified that the current core analysis methods can be applicable with good accuracy to core designs and safety analyses of such MOX LWR cores. On the other hand, it has been also recommended to extent the database for such validation including burned MOX cores.

A project was launched with support of the Ministry of Economy, Trade and Industry of Japan (METI) to ensure the validity of the current core analysis methods for the Full MOX ABWR cores and extent the database for future high burn up MOX LWR cores through the analyses of the PIE data, burn up credit critical experiments [1] and MOX core critical experiments. One of works of the project has started from the analysis of the PIE data of BWR UO_2 fuel to do preparatory works for the future analysis of MOX PIE data of the 1/3 MOX and the Full MOX ABWR cores and to extent the reference data to be compared with

* Corresponding author, Tel. +81-3-4511-1762, FAX +81-3-4511-1897, E-mail: yamamoto-toru@jnes.go.jp

the MOX fuel analysis.

This paper presents some results of the analysis of the PIE data of BWR fuel assemblies.

2. FP Rod-by-Rod Distribution in Assembly

2.1 Experimental Data

With the support of the METI, Nuclear Power Engineering Corporation (NUPEC) conducted post irradiation experiments of the lead-use-assemblies of BWR 8x8 high burn up fuel that was irradiate from 1989 to 1997 in the Unit 2 of Fukushima power station 2 (2F2) of Tokyo Electric Power Company (TEPCO). Comprehensive post irradiation examinations were applied for the five assemblies that were discharged after each cycle from the cycle 1 through the cycle 5. [2] The assembly average enrichment is 3.0 wt% and the burn ups were in the range of 13 to 48 GWd/t corresponding to the irradiation periods. The examinations include axial gamma ray spectrometry with a Ge(Li) detector that was performed for 16 fuel rods of the discharged UO2 bundles in a hot cell laboratory about 1 year after each cycle. Fig. 1 shows the rod location of measurements with the rod enrichment distribution and the fuel design data.

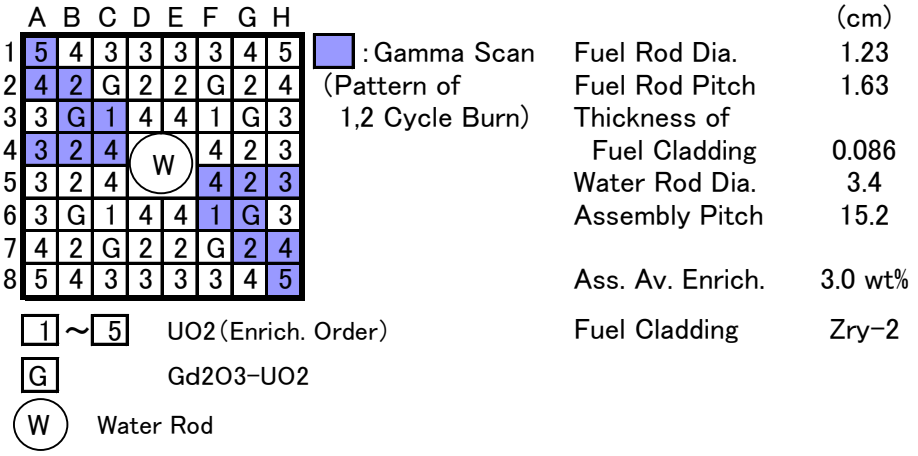

Fig. 1 Rod location of measurements with rod enrichment distribution and design data of BWR 8x8 high burn up fuel

By processing the intensity data of specific gamma rays from the decay of ^{137}Cs, ^{134}Cs, ^{109}Ru and ^{95}Zr the relative distributions of those FP nuclides in atomic number density were obtained in the axial direction of the 16 fuel rods. Table 1 summarizes the half-lives, fission yields, the specific gamma ray energies and the representing nuclear characteristics about the fuel burn up for those nuclides. From those data, the relative distributions of those FP nuclides among the 16 fuel rods were obtained for a typical top plain (in 15/24 to 18/24 node) and a bottom plain (in 3/24 to 6/24 node) of the fuel bundle. Fig. 2 shows an example of the relative distributions in the 18/24 node of the assembly discharged after the first cycle, which has the assembly average discharge burn-up of 12.6 GWd/t. The power and the exposure distribution is relatively smaller local variations except Gd_2O_3-UO_2 rods; however, the flux and the Pu accumulation have rather larger local variations reflecting the heterogeneity of the moderator density and enrichment distribution of the BWR assembly.

Table 2 shows the information of the fuel assembly, the discharged cycle, the assembly average discharge burn up, the nodes, for which the relative distributions of FP nuclides were compiled, and the node average burn up. The enrichment splitting of the assembly has 1/8

Table 1 Summary of characteristics of measured fission product nuclides

FP Nuclide	$T_{1/2}$[3]	Fission Yields % (Thermal Fission Cumulative)[4]	Gamma-ray energy keV [3]	Representing burn up characteristics
^{137}Cs	30.07 y	6.27 (^{235}U) 6.73 (^{239}P)	662	Exposure
^{134}Cs	2.0648 y	1.27E-5 (^{235}U) 9.89E-4 (^{239}P)	605 796	Exposure x flux
^{106}Ru	1.024 y	0.402 (^{235}U) 4.28 (^{239}P)	512(^{106}Rh)	Pu accumulation
^{95}Zr	64.02 d	6.50 (^{235}U) 4.89 (^{239}P)	757 724	Power

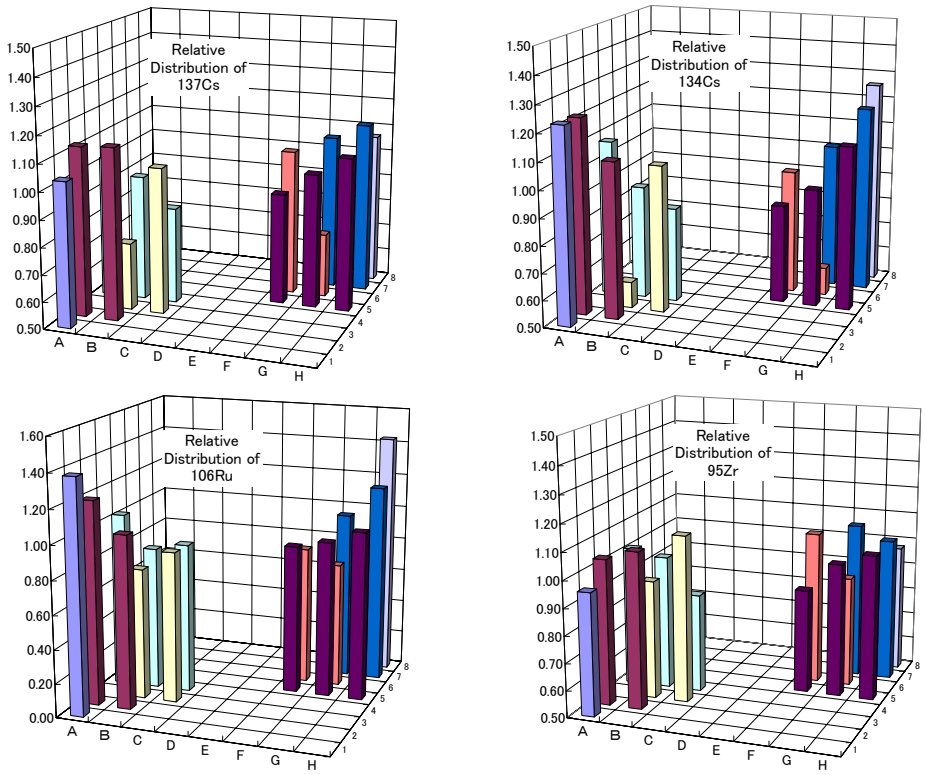

Fig. 2 Relative distributions of number densities of ^{137}Cs, ^{134}Cs, ^{109}Ru and ^{95}Zr among 16 fuel rods in a 18/24 node of an assembly with average discharge burn-up of 12.6 GWd/t

symmetry as shown in the Fig. 1 so that the FP distributions among the 16 rods are expected to have such symmetry. To check that symmetry, the average value was obtained for two symmetric positions, deviation from the average value was calculated in percentage and the root mean square (RMS) for the 8-rod positions was derived as an indicator of the overall symmetry. Table 3 shows the values of the RMS. Considering that each FP relative atomic densities are given a statistical error of 0.5 to 1 % for ^{137}Cs and ^{134}Cs, 1 to 1.5 % for ^{106}Ru and 1 to 3% for ^{95}Zr, relatively larger asymmetry was observed in ^{134}Cs ^{106}Ru and ^{95}Zr

of 2F2D8. This asymmetry is due to the gradient the thermal flux in the assembly that was loaded in the outermost core in the 5th cycle. Besides this special case in the loading position, there would be some other systematic influences on the symmetry caused by such as different characteristics of the adjacent assemblies in exposures, void fractions and others.

Table 2 List of relative distribution of FP data compiled

Assembly	Discharge Cycle	Assembly average discharge burn-up GWd/t	Upper node	Node average burn-up GWd/t	Lower node	Node average burn-up GWd/t
2F2D1	1	12.6	18/24	14.6	5/24	13.7
2F2D2	2	24.6	17/24	28.0	4/24	24.4
2F2D3	3	34.6	18/24	40.7	3/24	30.0
2F2D8	5	47.8	15/24	56.8	6/24	50.7

Table 3 Root mean square (RMS: %) of deviations from average values for 8 rod positions

Assembly	Discharge Cycle	^{137}Cs		^{134}Cs		^{106}Ru		^{95}Zr	
		Upper	Lower	Upper	Lower	Upper	Lower	Upper	Lower
2F2D1	1	1.86	0.87	1.96	2.70	2.46	2.04	1.23	1.26
2F2D2	2	1.87	0.81	1.36	1.40	2.07	2.21	2.39	2.14
2F2D3	3	2.53	0.96	1.00	2.02	3.20	2.50	4.11	6.60
2F2D8	5	1.42	1.19	5.66	1.39	6.37	2.29	18.23	3.43

For the following comparison between the calculation and the measurements of the FP densities, the average value for the 8 rod positions were used in order to reduce the systematic influence from adjacent fuel assemblies and the core gross gradient of neutron flux and to make them proper for comparison with the infinite assembly calculation mentioned in the following chapter.

2.2 Analysis Results

2.2.1 Analysis Methods

The burn-up calculations have been done using the Pij collision probability module coupled with burn-up calculation in the SRAC cord system. [5] The cross section library is a 107 energy group library installed in SRAC that was created from the nuclear data library JENDL-3.2. [6] The resonance library was produced by PEACO module where the hyperfine energy group calculation is done to treat resonance shielding in detail. The geometrical configuration is the one-fourth region of the 8x8 assembly considering the symmetry of the design with reflective boundary condition. A large center water rod was simulated by the four water rods with adjusting number densities of water and material. One material region was assigned to each UO_2 pellet and the ten material regions with a same volume to each Gd_2O_3-UO_2 fuel pellet.

The burn-up calculations have been done for 0, 40, 70 % in-channel void fractions up to 60 GWd/t. The time steps are 0.25 GWd/t up to 15 GWd/t where the effect of Gd_2O_3 almost disappears and 1.0 GWd/t after 15 GWd/t. The operating history data of the plant process computer gives the historical void fraction and the node average exposure for the corresponding node of the assembly. Interpolation has been done based on these calculations for the specific values of the historical void fraction and the node average

exposure.

2.2.2 Comparison Between Analysis Results and Measurements

Calculation results were compared with measurements of the nodes in Table 2. Fig. 3 shows the comparison for the relative distribution of number densities of ^{137}Cs, ^{134}Cs, ^{109}Ru and ^{95}Zr among 8 fuel rods in the 18/24 node with the node average burn-up of 13.7 GWd/t. The value of C-E (%) is from 1 to 3 % except for the Gd_2O_3-UO_2 fuel rod in (B, 3) position. Table 4 shows the root mean square of the difference between the analysis results and the measurements of the 7 rod positions excluding the Gd_2O_3-UO_2 fuel rod for each node. The difference, (C-E) x 100, is almost two times of the statistical errors of the measurements. This indicates the validity of the assembly calculation with present analysis methods since there would be some systematical uncertainties in the comparisons.

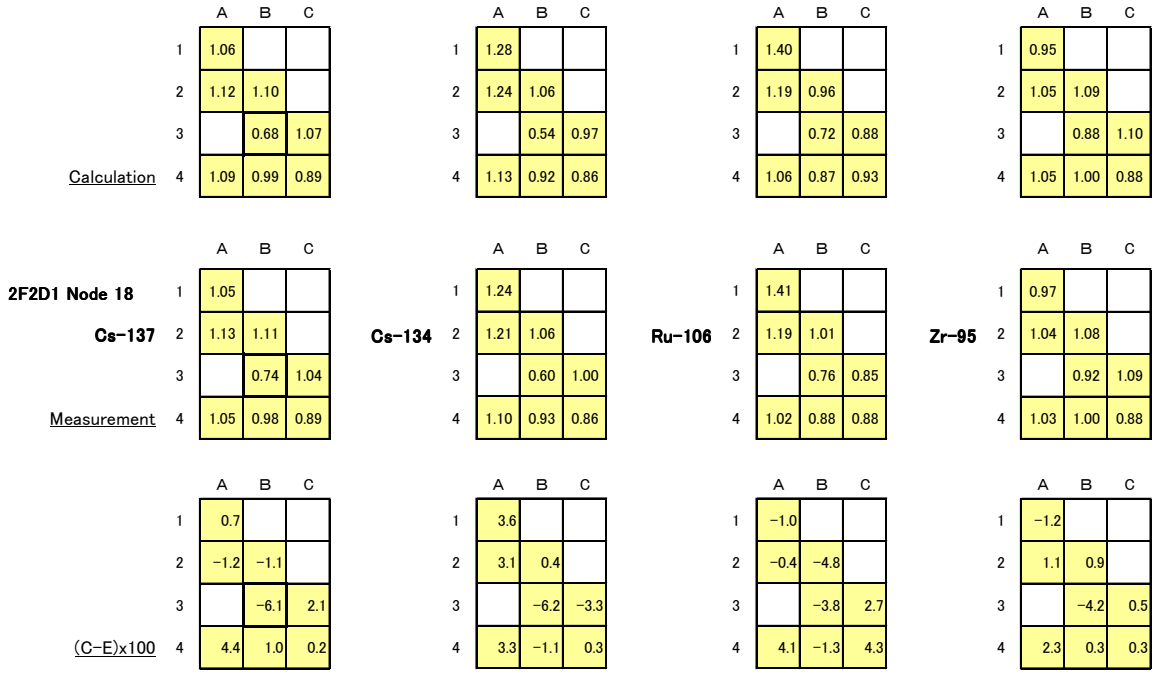

Fig. 3 Comparison between calculations and measured data for relative distributions of number densities of ^{137}Cs, ^{134}Cs, ^{109}Ru and ^{95}Zr among 16 fuel rods in 18/24 node for node average burn-up of 13.7 GWd/t

Table 4 Root mean square (RMS: %) of difference (C-E) between analysis results and measurements of 7 rod positions excluding Gd_2O_3-UO_2 fuel rod

Assembly	Discharge Cycle	^{137}Cs		^{134}Cs		^{106}Ru		^{95}Zr	
		Upper	Lower	Upper	Lower	Upper	Lower	Upper	Lower
2F2D1	1	2.01	1.75	2.43	2.37	3.14	1.63	1.16	2.25
2F2D2	2	2.03	1.82	2.18	4.13	3.18	2.09	2.43	2.12
2F2D3	3	1.16	1.36	2.20	2.57	3.49	3.53	2.96	2.93
2F2D8	5	1.43	1.22	1.31	2.29	3.56	1.22	6.23	5.93

2.3 Discussion

In the above comparison it was observed that the calculation underestimate by 6 to 2 % the measurements systematically for the Gd_2O_3-UO_2 fuel rod for every FP nuclides. This is

partly because that the fission reaction distribution and then the FP density distribution in the fuel pellets for this rod will be larger in the peripheral region of the rod than the UO_2 furl rod, which makes the relative FP density larger for the Gd_2O_3-UO_2 fuel rod if the proper correction is not applied for such effect. According to a preliminary study, such effect is evaluated to 3 to 1 % that makes reduce the discrepancy seen between the Gd_2O_3-UO_2 fuel rod and the UO_2 furl rod.

3. Rod Average Isotopic Composition

3.1 Experimental Data

With support of the Science and Technology Agency of Japan, Japan Atomic Energy Research Institute (JAERI) has performed a burn up credit research project entitled "The Technical Development on Criticality Safety Management of Spent LWR Fuels" since 1990. [7] This project includes the destructive analysis of the 18 spent-fuel samples from two BWR fuel rods, one UO_2 fuel rod of enrichment 3.9 wt% (SF89) and one Gd_2O_3-UO_2 fuel rod of enrichment 3.40 wt%- Gd_2O_3 4.5 wt% (SF99) from one fuel assembly that was irradiate 3 cycles in the 2F2 operated by TEPCO. The destructive analysis were performed for more than 40 nuclides of uranium, trans-uranium and fission product nuclides using radiochemical analysis cooperated mass spectrometry and alpha-ray and gamma-ray spectrometry. The burn up, which was determined by the ^{148}Nd method, is 4 to 44 GWd/t for the UO_2 fuel pellets and 7 to 37 GWd/t for the Gd_2O_3-UO_2 fuel pellets. Fig. 4 shows the rod location of measurements with the rod enrichment distribution and the fuel design data.

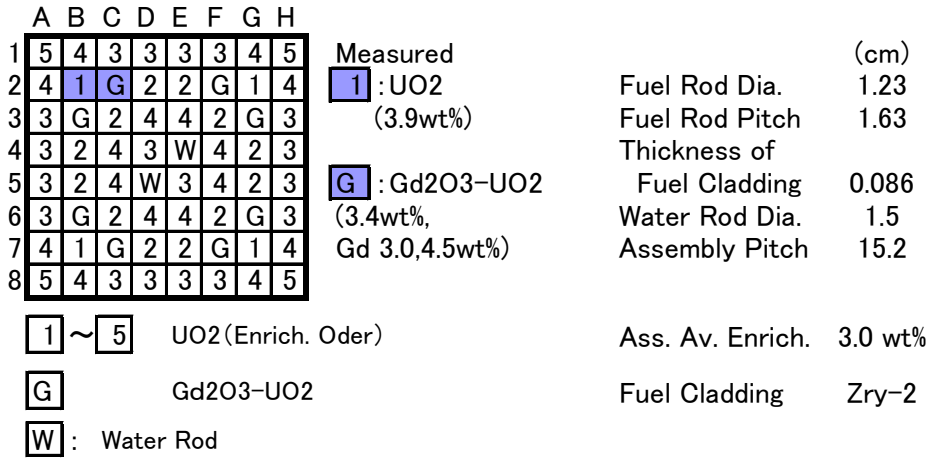

Fig. 4 Rod location of measurements with rod enrichment distribution and design data of BWR 8x8 fuel [7]

The measurement data will be shown in the next chapter for comparison with the lattice analysis calculation.

3. 2 Analysis Results

3.2.1 Analysis Methods

The burn-up calculations have been done using the same method explained in 2.2.1. Interpolation has been done based on these calculations for the specific values of historical void fraction and the measured pellet average exposure.

3.2.2 Analysis Results

The measured data and C/E is shown in Table 5 for SF98 (UO_2 fuel rod) and in Table 6 for

SF99 (Gd_2O_3-UO_2 fuel rod).

3.3 Discussion

The analysis of ^{235}U overestimates the measurements by 3 to 4 % that is larger than the measurement error of less than 0.1 %; however, the concentration of ^{235}U is sensitive to the pellet exposure, for which the measurement error is assigned as less than 3% and the calculation adopted the measurement value. The analysis of ^{236}U underestimates the measurements by 6 % that is larger than the measurement error of less than 2%. The analysis of ^{239}Pu and ^{240}Pu give good reproduction of the experiments. The discrepancy seen in ^{241}Pu and ^{241}Am would be caused by the simple treatment of cooling time in the analysis. The rather large discrepancy in the minor actinide nuclide and the fission product nuclides would be partly due to the difficulty in the measurements and the nuclear data and the simple treatment of the cooling time in the analysis. The detail evaluation of the discrepancy is necessary and now on going.

4. Conclusions

The calculations with the lattice analysis code have been done with the experimental data of the rod-by-rod distributions of the FP nuclide in the assemblies and the pellet average isotope compositions of actinide nuclides (U, Pu, Am and Cm) and the major FP nuclides. The experimental data were obtained from the PIE for the BWR 8x8 UO_2 fuel assemblies that were discharged from the Unit 2 of Fukushima power station 2 (2F2).

The SRAC cord system coupled with the JENDL-3.2 nuclear data library has been used for the burn-up calculations. For the rod-by-rod distributions of the FP nuclide, the value of C-E (%) is from 1 to 3 % except for the Gd_2O_3-UO_2 fuel rod. The root mean square of the difference between the analysis results and the measurements of the 7-rod positions excluding the Gd_2O_3-UO_2 fuel rod is almost in two times of the statistical errors of the measurements, which indicates the validity of the adopted lattice analysis. For the pellet average isotope compositions of actinide nuclides, the comparison results were discussed in terms of the measurement errors and the analysis methods. Further evaluation and discussion are necessary about the comparisons in the isotope compositions.

Acknowledgements

The authors express their appreciation to the advisory committee led by Prof. T. Takeda of the Osaka University for the technical advise and wish to thank Mr. M. Sasagawa of NUPEC and Mr. M. Yamamoto and Mr. M. Sugawara of the Global Nuclear Fuel - Japan for the collaboration in the analysis work.

References

1) P. Baeten et al., "The REBUS Experimental Programme for Burn-up Credit," Proc. Int. Conf. on Nuclear Critical Safety, ICNC2003, Tokai, Ibaraki, Japan, Oct. 20-24 (2003).
2) Y. Tsukuda et al., "Irradiation Behavior of LWR High Burnup Fuel," J. At. Energy Soc. Japan, **45**(11), 682 (2003).
3) Chart of the nuclides 2000, Japanese Nuclear Data Committee and Nuclear Data Center, JAERI (2000).
4) K. Tasaka, et al., "JNDC Nuclear Data Library of Fission Products - Second Version- , JAERI 1320 (1990).
5) K. Tsuchihashi et al., "Revised SRAC Code System," JAERI-1302 (1986).
6) T. Nakagawa et al. "JENDL-3.2," J. Nucl. Sci. Technol., **32**(12), 1259 (1995).

7) Y. Nakahara et al., "Nuclide Composition Benchmark Data Set for Verifying Burnup Codes on Spent Light Water Reactor Fuel," Nucl. Technol., **137**, 111 (2002).

Table 5 Measured number density* [7] (upper) and C/E for SF98 (UO_2 fuel rod) (bottom)

Sample	SF98-2	SF98-3	SF98-4	SF98-5	SF98-6	SF98-7	SF98-8	Av.C/E
GWd/t	26.51	36.94	42.35	43.99	39.92	39.41	27.18	–
Void(%)	0.0	3.0	11.0	32.0	54.5	68.0	73.0	–
^{234}U	2.677E+02	2.178E+02	1.976E+02	1.903E+02	1.860E+02	1.962E+02	2.354E+02	1.01
	0.96	1.01	1.00	1.00	1.07	1.00	1.01	
^{235}U	1.743E+04	8.142E+03	5.966E+03	6.315E+03	9.062E+03	9.357E+03	1.545E+04	1.03
	0.85	1.05	1.05	1.00	0.99	1.05	1.04	
^{236}U	3.551E+03	4.994E+03	5.284E+03	5.307E+03	5.140E+03	5.140E+03	4.291E+03	0.94
	1.10	0.95	0.95	0.95	0.94	0.94	0.92	
^{238}U	9.460E+05	9.406E+05	9.358E+05	9.328E+05	9.334E+05	9.332E+05	9.431E+05	1.00
	1.00	1.00	1.00	1.00	1.00	1.00	1.00	
^{237}Np	1.479E+02	3.346E+02	4.318E+02	3.862E+02	5.157E+02	4.573E+02	2.918E+02	1.04
	1.40	1.02	0.98	1.23	0.90	1.06	1.03	
^{238}Pu	2.827E+01	1.167E+02	1.678E+02	1.936E+02	1.692E+02	2.083E+02	9.544E+01	0.89
	1.42	0.85	0.88	0.94	1.02	0.89	0.78	
^{239}Pu	3.372E+03	3.694E+03	3.792E+03	4.265E+03	5.305E+03	5.628E+03	5.341E+03	0.99
	1.08	0.99	0.98	0.98	0.95	1.01	1.02	
^{240}Pu	1.121E+03	2.135E+03	2.458E+03	2.613E+03	2.630E+03	2.668E+03	1.816E+03	0.98
	1.35	1.00	0.98	0.98	0.96	0.97	0.98	
^{241}Pu	4.308E+02	8.949E+02	1.032E+03	1.172E+03	1.292E+03	1.355E+03	9.079E+02	0.97
	1.41	0.97	0.96	0.97	0.95	0.97	0.99	
^{242}Pu	9.292E+01	4.623E+02	6.622E+02	6.939E+02	5.431E+02	5.439E+02	2.220E+02	0.93
	1.82	0.92	0.92	0.96	0.96	0.91	0.92	
^{241}Am	2.300E+01	3.271E+01	3.417E+01	3.734E+01	4.091E+01	4.388E+01	3.295E+01	1.20
	0.86	1.04	1.20	1.31	1.34	1.38	0.95	
^{242m}Am	2.967E-01	4.999E-01	5.298E-01	6.417E-01	8.623E-01	8.975E-01	7.074E-01	0.89
	0.78	0.83	0.94	0.99	0.91	1.01	0.64	
^{243}Am	6.991E+00	6.678E+01	1.138E+02	1.273E+02	1.116E+02	1.087E+02	3.259E+01	0.89
	2.19	0.85	0.85	0.95	0.87	0.92	0.90	
^{242}Cm	3.581E+00	1.696E+01	2.263E+01	3.460E+01	5.925E+01	2.892E+01	1.153E+01	0.50
	1.13	0.60	0.63	0.48	0.25	0.53	0.53	
^{243}Cm	3.710E-02	3.135E-01	4.247E-01	4.946E-01	5.347E-01	5.932E-01	2.073E-01	0.61
	1.21	0.55	0.67	0.75	0.63	0.61	0.47	
^{244}Cm	8.003E-01	1.696E+01	3.635E+01	4.999E+01	4.229E+01	4.484E+01	8.687E+00	0.75
	2.67	0.74	0.75	0.78	0.73	0.75	0.73	
^{245}Cm	1.646E-02	5.485E-01	1.338E+00	2.322E+00	2.480E+00	2.734E+00	3.928E-01	0.79
	3.52	0.81	0.81	0.82	0.73	0.80	0.77	
^{246}Cm	No data	7.666E-02	2.311E-01	3.850E-01	2.935E-01	3.007E-01	1.635E-02	0.67
	No data	0.62	0.65	0.66	0.58	0.63	0.90	
^{143}Nd	7.567E+02	8.234E+02	8.486E+02	9.039E+02	9.199E+02	9.183E+02	7.358E+02	1.01
	0.94	1.02	1.03	1.01	1.00	1.01	1.00	
^{144}Nd	8.511E+02	1.275E+03	1.492E+03	1.476E+03	1.284E+03	1.207E+03	7.478E+02	1.02
	0.86	0.97	1.02	1.07	1.03	1.05	0.96	
^{145}Nd	5.974E+02	7.648E+02	8.423E+02	8.667E+02	7.950E+02	7.845E+02	5.770E+02	1.02
	0.98	1.02	1.03	1.02	1.02	1.02	1.01	
^{146}Nd	5.278E+02	7.629E+02	8.916E+02	9.320E+02	8.427E+02	8.330E+02	5.550E+02	0.99
	1.00	0.99	0.99	0.99	0.98	0.98	0.99	
^{148}Nd	2.905E+02	4.058E+02	4.662E+02	4.850E+02	4.407E+02	4.356E+02	2.997E+02	1.00
	1.01	1.00	1.00	1.00	1.00	1.00	1.00	
^{150}Nd	1.279E+02	1.867E+02	2.193E+02	2.294E+02	2.098E+02	2.080E+02	1.389E+02	1.00
	1.01	1.00	0.99	1.00	0.99	0.99	0.99	
^{137}Cs	8.286E+02	1.329E+03	1.577E+03	1.588E+03	1.508E+03	1.559E+03	9.494E+02	0.99
	1.18	1.01	0.97	1.00	0.96	0.92	1.05	
^{134}Cs	3.214E+01	1.010E+02	1.407E+02	1.553E+02	1.514E+02	1.621E+02	6.979E+01	0.90
	1.63	0.96	0.90	0.90	0.83	0.79	1.00	
^{154}Eu	6.857E+00	1.818E+01	2.413E+01	2.601E+01	2.931E+01	2.924E+01	1.708E+01	0.74
	1.14	0.75	0.71	0.77	0.70	0.77	0.74	
^{144}Ce	1.833E+02	2.996E+02	3.538E+02	4.107E+02	3.520E+02	3.786E+02	2.867E+02	0.86
	1.68	1.02	0.84	0.71	0.82	0.76	1.03	
^{125}Sb	No data	No data	No data	No data	5.223E+00	No data	Nodata	1.40
	No data	No data	No data	No data	1.40	No data	No data	
^{106}Ru	4.985E+01	1.091E+02	1.237E+02	1.326E+02	1.113E+02	1.309E+02	7.522E+01	1.17
	1.74	1.12	1.15	1.13	1.24	1.06	1.35	
^{147}Sm	2.303E+02	3.091E+02	3.207E+02	3.025E+02	2.891E+02	2.800E+02	2.454E+02	0.94
	1.00	0.91	0.93	0.98	0.96	0.96	0.88	
^{148}Sm	5.771E+01	1.531E+02	1.971E+02	2.022E+02	1.855E+02	1.852E+02	1.079E+02	1.16
	2.25	1.21	1.10	1.13	1.12	1.11	1.28	
^{149}Sm	2.201E+00	2.553E+00	2.502E+00	3.701E+00	3.374E+00	4.199E+00	4.082E+00	0.78
	1.09	0.88	0.87	0.63	0.81	0.72	0.79	
^{150}Sm	1.790E+02	3.309E+02	3.865E+02	3.808E+02	3.536E+02	3.505E+02	2.408E+02	0.92
	1.17	0.89	0.88	0.94	0.93	0.94	0.93	
^{151}Sm	8.203E+00	9.192E+00	9.738E+00	1.039E+01	1.272E+01	1.310E+01	1.245E+01	0.95
	1.04	0.94	0.92	0.97	0.92	0.99	0.98	
^{152}Sm	9.016E+01	1.425E+02	1.555E+02	1.432E+02	1.233E+02	1.222E+02	9.771E+01	1.14
	1.25	1.07	1.09	1.19	1.23	1.20	1.09	
^{154}Sm	1.874E+01	3.950E+01	4.828E+01	4.912E+01	4.377E+01	4.472E+01	2.933E+01	0.88
	1.16	0.86	0.86	0.90	0.91	0.89	0.84	

*Unit: g/TIHM (Ton Initial Heavy Metal)

Table 6 Measurement number density* [7] (upper) and C/E for SF99 (Gd_2O_3-UO_2 fuel rod) (bottom)

Sample	SF99-2	SF99-3	SF99-4	SF99-5	SF99-6	SF99-7	SF99-8	SF99-9	Av.C/E
GWd/t	22.63	32.44	35.42	37.41	32.36	32.13	21.83	16.65	–
Void(%)	1.4	5.8	10.8	27.7	54.7	66.5	71.7	72.9	–
^{234}U	2.006E+02	1.782E+02	1.666E+02	1.602E+02	1.649E+02	1.643E+02	1.960E+02	2.184E+02	1.07
	1.10	1.06	1.07	1.06	1.09	1.08	1.07	1.04	
^{235}U	1.398E+04	8.657E+03	6.981E+03	7.381E+03	1.046E+04	1.092E+04	1.575E+04	1.906E+04	1.04
	1.04	1.02	1.08	0.98	1.03	1.04	1.05	1.05	
^{236}U	3.467E+03	4.251E+03	4.480E+03	4.522E+03	4.295E+03	4.251E+03	3.458E+03	2.833E+03	0.94
	0.94	0.96	0.95	0.96	0.94	0.94	0.93	0.94	
^{238}U	9.522E+05	9.452E+05	9.432E+05	9.394E+05	9.409E+05	9.403E+05	9.493E+05	9.538E+05	1.00
	1.00	1.00	1.00	1.00	1.00	1.00	1.00	1.00	
^{237}Np	2.177E+02	3.632E+02	3.666E+02	4.617E+02	4.146E+02	4.464E+02	2.758E+02	1.975E+02	0.87
	0.84	0.84	0.95	0.86	0.90	0.87	0.87	0.85	
^{238}Pu	3.961E+01	9.696E+01	1.145E+02	1.234E+02	1.374E+02	1.377E+02	6.476E+01	3.427E+01	0.97
	0.92	0.93	1.00	1.17	0.94	1.02	0.88	0.90	
^{239}Pu	3.907E+03	3.980E+03	3.865E+03	4.549E+03	5.633E+03	6.036E+03	5.448E+03	4.731E+03	1.00
	0.97	0.97	1.01	0.94	0.96	1.00	1.03	1.09	
^{240}Pu	1.519E+03	2.131E+03	2.293E+03	2.535E+03	2.445E+03	2.487E+03	1.647E+03	1.182E+03	0.99
	0.99	0.99	1.00	0.97	0.97	0.98	1.00	1.04	
^{241}Pu	6.763E+02	9.452E+02	1.010E+03	1.196E+03	1.263E+03	1.313E+03	8.332E+02	5.372E+02	0.96
	0.91	0.95	0.97	0.92	0.93	0.95	0.99	1.09	
^{242}Pu	1.896E+02	4.374E+02	5.573E+02	6.073E+02	4.334E+02	4.215E+02	1.723E+02	8.334E+01	0.91
	0.84	0.90	0.88	0.92	0.91	0.91	0.91	0.99	
^{241}Am	2.110E+01	3.950E+01	5.410E+01	4.363E+01	4.558E+01	4.848E+01	3.619E+01	2.885E+01	0.92
	0.95	0.89	0.74	1.09	1.15	1.19	0.79	0.57	
^{242m}Am	4.239E-01	5.444E-01	3.418E-01	6.917E-01	9.306E-01	9.240E-01	6.812E-01	4.078E-01	0.83
	0.56	0.80	1.45	0.90	0.83	0.96	0.61	0.55	
^{243}Am	1.895E+01	6.496E+01	9.037E+01	1.128E+02	8.514E+01	8.453E+01	2.574E+01	9.255E+00	0.83
	0.77	0.83	0.82	0.84	0.81	0.84	0.82	0.93	
^{242}Cm	1.624E+01	2.270E+01	3.477E+01	6.130E+01	3.844E+01	4.067E+01	1.593E+01	5.534E+00	0.33
	0.24	0.44	0.35	0.24	0.32	0.31	0.31	0.43	
^{243}Cm	9.310E-02	2.759E-01	3.692E-01	4.750E-01	4.413E-01	4.762E-01	1.629E-01	7.257E-02	0.54
	0.48	0.61	0.62	0.64	0.58	0.59	0.46	0.38	
^{244}Cm	3.180E+00	1.645E+01	2.692E+01	3.871E+01	3.008E+01	3.000E+01	6.152E+00	1.515E+00	0.72
	0.65	0.73	0.71	0.73	0.66	0.72	0.69	0.86	
^{245}Cm	8.762E-02	5.695E-01	1.014E+00	1.767E+00	1.735E+00	1.793E+00	2.702E-01	8.185E-02	0.71
	0.66	0.78	0.76	0.77	0.66	0.78	0.73	0.57	
^{246}Cm	No data	6.949E-02	1.495E-01	2.412E-01	1.603E-01	1.561E-01	1.441E-02	1.217E-02	0.54
	No data	0.66	0.61	0.67	0.54	0.62	0.56	0.11	
^{247}Cm	No data	1.427E-03	No data	2.809E-03	No data	3.881E-03	No data	1.224E-02	0.27
	No data	0.23	No data	0.57	No data	0.28	No data	0.00	
^{143}Nd	6.136E+02	7.627E+02	7.808E+02	8.397E+02	7.984E+02	8.089E+02	6.143E+02	5.007E+02	0.99
	1.00	0.99	1.01	0.98	1.00	1.00	0.99	0.97	
^{144}Nd	6.537E+02	1.321E+03	1.203E+03	1.166E+03	9.321E+02	8.171E+02	5.531E+02	4.406E+02	0.95
	0.88	0.77	0.97	1.06	1.03	1.14	0.95	0.78	
^{145}Nd	4.917E+02	6.728E+02	7.198E+02	7.511E+02	6.519E+02	6.509E+02	4.671E+02	3.705E+02	1.01
	1.02	1.01	1.02	1.01	1.02	1.01	1.01	0.99	
^{146}Nd	4.476E+02	6.610E+02	7.314E+02	7.774E+02	6.671E+02	6.645E+02	4.397E+02	3.307E+02	0.99
	1.00	0.99	0.99	0.99	0.98	0.98	0.99	0.99	
^{148}Nd	2.486E+02	3.570E+02	3.903E+02	4.130E+02	3.575E+02	3.556E+02	2.411E+02	1.837E+02	1.00
	1.01	1.00	1.00	1.00	1.00	1.00	1.00	1.01	
^{150}Nd	1.142E+02	1.674E+02	1.844E+02	1.979E+02	1.735E+02	1.724E+02	1.136E+02	8.436E+01	1.00
	1.00	1.00	1.00	1.00	0.99	1.00	1.00	1.01	
^{137}Cs	8.515E+02	1.231E+03	1.346E+03	1.427E+03	1.249E+03	1.266E+03	8.343E+02	6.329E+02	0.96
	0.98	0.96	0.96	0.95	0.94	0.92	0.96	0.98	
^{134}Cs	4.643E+01	9.117E+01	1.126E+02	1.306E+02	1.137E+02	1.193E+02	5.684E+01	3.213E+01	0.87
	0.91	0.90	0.86	0.84	0.80	0.78	0.88	0.98	
^{154}Eu	1.022E+01	1.792E+01	1.992E+01	2.465E+01	2.549E+01	2.659E+01	1.404E+01	8.215E+00	0.70
	0.67	0.70	0.73	0.69	0.67	0.70	0.71	0.75	
^{144}Ce	2.153E+02	No data	2.915E+02	3.847E+02	3.169E+02	4.240E+02	2.540E+02	1.657E+02	0.98
	1.29	No data	0.98	0.73	0.84	0.62	1.00	1.43	
^{125}Sb	3.674E+00	4.205E+00	4.588E+00	4.667E+00	5.071E+00	3.837E+00	2.430E+00	1.234E+00	1.67
	1.22	1.48	1.47	1.52	1.26	1.67	1.88	2.88	
^{106}Ru	3.280E+01	8.056E+01	7.833E+01	6.988E+01	6.899E+01	4.985E+01	4.366E+01	5.029E+01	1.92
	2.56	1.47	1.65	1.96	1.78	2.48	2.04	1.39	
^{147}Sm	No data	2.609E+02	No data	2.770E+02	No data	2.436E+02	1.965E+02	1.633E+02	0.98
	No data	1.01	No data	1.00	No data	1.00	0.96	0.95	
^{148}Sm	No data	1.167E+02	No data	1.579E+02	No data	1.343E+02	7.545E+01	4.483E+01	1.48
	No data	1.43	No data	1.25	No data	1.28	1.51	1.91	
^{149}Sm	No data	2.469E+00	No data	2.723E+00	No data	3.426E+00	2.959E+00	2.600E+00	1.00
	No data	0.91	No data	0.87	No data	0.91	1.08	1.22	
^{150}Sm	No data	2.676E+02	No data	3.246E+02	No data	2.778E+02	1.830E+02	1.313E+02	0.98
	No data	0.98	No data	0.95	No data	0.97	0.98	1.02	
^{151}Sm	No data	8.490E+00	No data	1.025E+01	No data	1.294E+01	1.155E+01	9.999E+00	1.03
	No data	1.01	No data	0.95	No data	1.01	1.04	1.14	
^{152}Sm	No data	1.179E+02	No data	1.272E+02	No data	1.024E+02	7.730E+01	6.172E+01	1.17
	No data	1.16	No data	1.18	No data	1.22	1.15	1.12	
^{154}Sm	No data	3.353E+01	No data	4.215E+01	No data	3.579E+01	2.211E+01	1.540E+01	0.94
	No data	0.94	No data	0.92	No data	0.94	0.94	0.97	

*Unit: g/TIHM (Ton Initial Heavy Metal)